RSC Advances

ROYAL SOCIETY OF CHEMISTRY

www.rsc.org/advances

Graphical abstract

Control of size, morphology and dispersability in water of boehmite nanoparticles prepared with additives by a hydrothermal via

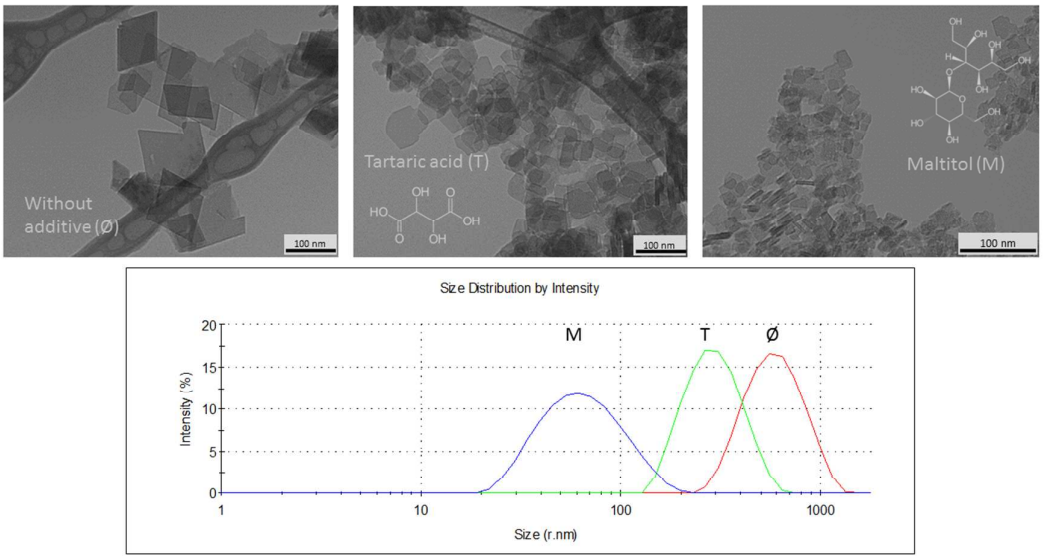

Improvement of boehmite nanoparticles aqueous dispersability by controlling their size, shape and crystallinity

Pablo Pardo, José Miguel Calatayud and Javier Alarcón

University of Valencia, Department of Inorganic Chemistry, Calle Doctor Moliner 50, 46100-Burjasot (Valencia), Spain

Introduction

Nanocrystals with different shapes have been extensively studied during the last two decades because they allowed developing materials with new properties and potential new applications in as different fields as catalysis, biomedicine or ceramics [1, 2, 3]. One type of nanoparticles of great interest is the one based in aluminum oxohydroxide and more specifically the γ-AlOOH polymorph, named boehmite, both because its role as a precursor of γ-Al_2O_3, a catalyzer support quite used in the petrochemical industry and also as a support of molecules and/or biomolecules with specific functionalities in different media[4, 5, 6]. The structure of boehmite consists of $Al(O,OH)_6$ units forming octahedral layers by sharing edges. Layers are stacked in [010] direction, linked by hydrogen bonds. The most accepted space group is *Cmcm*, with cell parameters a=2.86, b=12.21 and c=3.69[7]. Depending on the preparation conditions different nanoparticle morphologies are obtained[7], with four types of exposed surfaces, namely the (100), (010), (001) and (101), whose different prevalence determines the physical-chemical properties of the material. Recently, we reported the functionalization of boehmite nanoparticles with different molecules to develop potential sensors of cations and anions in aqueous solution by fluorescent spectroscopy as well as potential contrast agents for NMR imaging[8, 9]. The good performance of these supported molecules into the boehmite surface is caused by the non-aggregation of nanoparticles in a range of pH. The stability of the aqueous dispersions allowed performing in situ emission measurements in solution because the colloidal particles did not produce any scattering. It is also well known that the boehmite has been used for long as adjuvant in practically all high-volume vaccines, being in safe use as such for many years[10]. All these contrasted abilities of boehmite nanoparticles allow forecasting their potential use after functionalization. However, the preparation of stable dispersions of well-shaped,

monosized boehmite nanocrystals in a wide pH window is necessary for improving their applicability.

Three are the preparation methods usually used in the synthesis of boehmite nanoparticles in aqueous solution. The precipitation from aqueous aluminum solutions has been widely used but it requires a strict control of many reaction parameters[11]. The hydrolysis and condensation of aluminum alkoxides followed by peptization in acid media has also allowed obtaining boehmite[12]. However, the dispersion stability in aqueous solution of the obtained boehmites decreases on increasing pH, i. e. pH > 9, and the sol solution transform in a gel. The hydrothermal via has been also been extensively utilized in the preparation of boehmites in aqueous solution[13, 14, 15, 16]. Some additives (or ligands) such as polyols, polycarboxylic acids, anions, and different surfactants have been used with the goal of controlling the size, morphology and even the dispersability of boehmite nanoparticles in aqueous solution[17, 18, 19, 20, 21, 22, 23]. It has been proved that the efficiency of acyclic polyols as complexing agents depends on both the number of OH groups bonded to the carbon chain and their stereochemistry[17]. This ability causes a modification of the usual morphologies observed for boehmite nanoparticles, specifically resulting in an increase of (101) faces area. In order to check the effect of a large-volume polyol, in which the stabilization of boehmite colloidal dispersions would have a steric component, in this work maltitol was chosen as additive in the hydrothermal preparation of boehmite. The influence of some organic acids on the synthesis of boehmite has also been reported[20]. The role of these additives is proposed to be complete inhibition of gibbsite formation and facilitation of boehmite nucleation through different extent of complex formation by multidentate ligands. In our view, to compare the effect of a carboxylic acid, such as the tartaric acid, with a

large-volume polyol, on the size, morphology and aqueous dispersability of boehmites prepared by the hydrothermal via is worthy.

According to the reported data, two distinct boehmite morphologies can be obtained after hydrothermal processing of the precipitated solid (xerogel) depending on the pH of the starting solution. Although boehmite is the main crystalline phase detected in those precipitates, bayerite and/or gibbsite have also been found[24]. Boehmite nanocrystals are fibers in acidic conditions (pH=2-5) whereas plates under basic media pH=(10-11)[25, 26, 27, 28]. Results also showed that boehmite nanocrystal final sizes are mainly dependent on the temperature and time of the hydrothermal process. The higher the temperature and/or longer processing time, the larger the size of boehmite nanocrystals is. However, no quantitative evaluation on the size variation has been reported so far.

In order to avoid the presence of any aluminum hydroxide in the precipitate and on the contrary favor the precipitation of boehmite as only crystalline phase in the first solid, some authors stated that precipitation should be carried out in hot aqueous solution[29, 30]. Thus, the first goal in this paper is to evaluate the effect of temperature and time of the hydrothermal processing of xerogels obtained at 100 ºC on the morphology, size and aqueous dispersion stability of final boehmites. Moreover, we intend to evaluate the effect of two additives, a large-volume polyol as maltitol and a carboxylic acid as tartaric acid, present in the aqueous solution before the precipitation of boehmite at the first step, on the final size and morphology of boehmite as a function of the temperature and time of the hydrothermal processing. Also, the aqueous dispersability of boehmites prepared with and without additives will be compared.

Experimental section

Preparation procedure

Preparation of boehmite nanoparticles proceeded in aqueous media, through the precipitation of a gel by the alkalization of a solution of aluminum nitrate and its subsequent hydrothermal aging. The synthetic methodology is based on the general procedure previously used by several authors[17]. Besides extending the temperature range of the hydrothermal aging, the procedure applied in this study performed the precipitation step at high temperature, i. e. 100 ºC, conditions which were reported to favor the formation of boehmite among other aluminum hydroxide phases in non-aqueous routes[29]. The effect of two additives, tartaric acid and maltitol, in the final morphology and microstructure, and aqueous dispersion stability of boehmites was tested versus the material obtained without additive.

An initial 0.1 M $Al(NO_3)_3 \cdot 9H_2O$ (Panreac) solution (pH ca. 2) was heated to 100 ºC under stirring in a reflux system. In the preparations with additive, 0.01 mol/L of tartaric acid ($C_4H_6O_6$, Sigma-Aldrich) or maltitol ($C_{12}H_{24}O_{11}$, Sigma-Aldrich) were added in the initial solution. Once the temperature was reached, NaOH 5 M was dropwise added until adjusting pH = 10. A white, dense precipitate of boehmite was formed during the addition. The so-obtained precipitate was then hydrothermally aged for 24, 72 and 168 h at two different temperatures. For the treatments at 150 ºC, 100 mL PTFE vessels were used, meanwhile the aging at 200 ºC was carried out in PTFE lined stainless steel autoclaves. After the hydrothermal aging, which occurred without pH variation, samples were centrifuged and washed in water for three times. Hydrogels were finally dried overnight in a furnace at 100 ºC. Assuming the quantitative precipitation of boehmite from the aluminum nitrate initial solution yields of ca. 65% where achieved after the complete procedure. Materials were labeled X_YYY_ZZZ, where X indicates the absence of additive (0) or the use of tartaric acid (T) or maltitol (M), and YYY and ZZZ

correspond to the temperature and time -in hours- of the hydrothermal treatment, respectively.

Materials characterization

Characterization was mainly focused on the morphological and microstructural features of the boehmite nanoparticles and on the properties of their aqueous suspensions.

The size and shape of the final nanoparticles were observed by transmission electron microscopy (TEM) at 100 kV (Model 1010, Jeol, Tokyo, Japan). Samples were prepared by dispersing as-produced powders in water and setting a drop of the suspensions on copper grids that had previously been coated with a holey thin carbon film. The size of boehmite nanoparticles was determined by randomly selecting between 225 and 50 nanoparticles from the TEM images and manually measuring the major diagonal of their base by using the Image J software. Likewise, the particle thicknesses were measured by the occurrence of edgewise lying particles. In a typical measurement, a ratio of 4 pixels/nm was set from the resolution to magnification ratio of the image. From the set of measurements histograms were generated to determine the full width at half maximum (FWHM) of the particle length (size) distributions. Aspect ratio of the nanoparticles was calculated dividing the average diagonal length by the corresponding average thickness.

HRTEM images were collected using a Tecnai G2 F20 field emission electron microscope operating at 200 kV and equiped with a Gatan CCD camera. Samples were also prepared by evaporation of very dilute aqueous suspensions onto carbon-coated grids. Data treatment was performed with Digital Micrograph software.

XRD analysis of powder samples were performed in a Bruker D-8 Advance diffractometer, using Cu K_α radiation, with 1 and 3 mm divergence and antiscattering slits respectively and a 3º 2θ range Lynxeye linear detector. The X-ray powder diffraction patterns were run from 5 to 80º 2θ with a step size of 0.02º 2θ and an accumulated counting time of 0.2 s. EVA software was used for profile analysis and application of Scherrer's equation (λ= 1.541874 Å; K=1) for the determination of crystallite size in different crystallographic directions.

Elemental analysis was carried out in a CE Instruments EA1110 Elemental Analyzer, set for the detection of Nitrogen, Carbon and Hydrogen, using atropine as standard.

Particle size distribution (PSD) of the suspensions prepared by dispersion in water of the obtained powders was measured by dynamic light scattering in a Zetasizer Nano ZS (Malvern Instruments) equipment. Stable, suitable for measurement 0.3 g/L dispersions of boehmite were obtained by sonication (10 s., 150 W) and subsequent adjustment of pH = 10 with NaOH. The same equipment was used in the measurements of ζ-potential in 0.1 g/L suspensions of boehmite nanoparticles adjusted at pH=8.7.

Results and discussion

Electron Microscopy Observations

TEM images in Figure 1 summarize the most significant morphological features of the samples prepared in this study. Left column shows micrographs of no-additive preparations; middle and right columns correspond to procedures with addition of tartaric acid and maltitol, respectively. In rows, different conditions of hydrothermal synthesis are displayed; from up to bottom, 150 ºC (24 h and 168 h), 200 ºC (24 h and 168 h). As it can

be seen in Figure 1, the size and shape of the boehmite nanoparticles were strongly influenced by the presence of additive as well as by the time and temperature of the hydrothermal treatment over the range of experimental conditions used in this study. It is to note that the scale bars in Figure 1 are of 100 nm for all micrographs but J, K, and L, which are 200 nm long.

For free-additive prepared boehmites particle size increased with the temperature and holding time of the treatment. This fact can be observed for samples 0_150_24, 0_150_168, 0_200_24 and 0_200_168 in the micrographs shown in Figure 1 A, D, G and J. The PSDs calculated from length measurements on TEM images shown in Table 1 and Figure 1S shifted to greater size values and broadened over a wider range as time and temperature increased. The relatively small boehmites obtained at 150 ºC for 24 h showed sizes between ca. 14-26 nm. On increasing the temperature up to 200 ºC during 24 h the size range increased to values between ca. 45-95 nm. After 168 h at 200 ºC, the boehmite nanoparticles showed sizes in the range ca. 70-120 nm.

Regarding the effect of the presence of additive, it can be easily observed from the variations in the materials obtained at 200 ºC, where differences between samples are notably larger than in preparations at 150 ºC, although same trends were preserved. Particles in sample 0_200_24 (Figure 1G) consisted in well-defined diamond-shaped platelets with sharp edges forming angles of 104º and 76º. Same morphology was described for commercial[31] and basic-media obtained boehmite nanoparticles[17]. Nevertheless, particles obtained in the presence of additive (1H, 1I) exhibited rather square morphologies, with angles closer to 90º. These differences were not so clear in samples obtained at 150ºC, 24 h (Figure 1 upper row, 1A vs. 1B-1C) but for materials prepared at 200ºC for 168 h were even more pronounced (Figure 1 bottom row, 1J vs 1K-1L). Regarding size, and based on measurements of the major diagonal of the particles

performed on the TEM images, average length of the particles decreased in the sequence 0>T>M. Table 1 resumes the main descriptive parameters of the size distributions calculated from TEM measurements, represented in Figure 1S. Distributions shifted their maxima towards lower values of length while narrowing their respective widths (FWHM), also in the sequence 0-T-M, for all analysed series of samples. From those values and from the direct observation of the distributions in Figure 1S, it can be stated that the presence of additives resulted in a ca. 40 % of reduction in size of the particles for tartaric acid and of ca. 80 % for maltitol. The presence in the micrographs of samples obtained at 200ºC of some edgewise lying particles allowed the observation and measurement of thicknesses. Average values obtained together with the total numbers of measurements are also shown in Table 1. These measurements allowed the calculation of the aspect ratio (r) of the particles as the ratio of their major diagonal to their thickness.

As can be observed in Table 1 the studied additives presented different effect on the final shape of the nanoparticles. Tartaric acid route yielded particles of similar, constant aspect ratio of those obtained without additive (ca. 4, Table 1). Nevertheless, particles obtained with maltitol showed lower values of aspect ratio which, furthermore, decreased with hydrothermal treatment time (from 3.3 to 2.3). In agreement with this, previous works found in the literature observed that the presence of additives of polyol type in the preparation of boehmite led to the increase of the amount of particle lateral surfaces (i.e. (100), (001) and (101)) relative to basal planes, as a result of either a lateral surface stabilization induced by the presence of xylitol through adsorption or by the lowering of crystal growth kinetic[18]. The thermodynamic adsorption of xylitol described in the mentioned study and of other acyclic polyols of 2 to 6 carbon atoms in their backbone included in a later work[17] was reported to happen preferentially in the lateral faces, where cavities containing –OH groups in the structure of boehmite stabilized the interaction with

the polyols through hydrogen bonds. This so-called "nest effect" favoured the stabilization of lateral faces leading to their higher morphological expression in the final particles. The extent of this effect also depended on the complexing strength of the polyol, greatly affected by its stereochemistry. In the present work, maltitol was carefully chosen among other polyols in order to study the effect of its voluminous structure (12 carbon atoms including a pyran cycle) on the final particle size and on the stability of the aqueous suspensions of nanoparticles. Previous results on other polyols were obtained in soft hydrothermal experiments at 95 ºC[17] so direct comparison could be misleading. Still, maltitol allowed to restrain the size of the nanoparticles when higher hydrothermal temperatures were used, thus helping to achieve well-crystallized nanomaterials.

Tartaric acid, on its side, seems to present a different role in the synthesis of boehmite nanoparticles. Tartrate anion present in the solution at alkaline conditions is constituted by two planar halves with the four carbon atoms lying in a plane, each half containing a carboxyl group, tetrahedral carbon and hydroxyl oxygen atom[31]. With this configuration, tartrate anion can coordinate Al^{3+} to form different tartrate-aluminum complex anions depending on the pH[32]. At high pH values as the ones used in this work the formation of the binuclear specie $[Al_2 (C_4O_6H_2)_2]^{2-}$ (log β= -18.95) competed with the tetrahydroxyl-aluminium (III) ($[Al (OH)_4]^-$ (log β= -23.46)[32] among the other aquohydroxo complexes $[Al(OH)_h(OH_2)_{6-h}]^{(3-h)+}$ involved in condensation through the olation/oxolation mechanism[33], thus hindering Al^{3+} polymerization, and consequently slowing down boehmite formation, reported in the literature[14] to increase over pH 5 in hydrothermal aging by the enhancement of the dissolution-reprecipitation reaction. Due to their smaller size, particles obtained with the tartaric acid addition had higher specific surface area, thus higher proportion of lateral faces than additive-free nanoparticles with the same aspect ratio, a reported effect of the lowering of crystal growth kinetic[18].

Temperature of hydrothermal aging, as expected, increased the particle size of the materials. Remarkably developed shapes and sizes were achieved when working at 200 ºC compared to the results of procedures at 150 ºC. In contrast, the main effect of holding time of treatment on the samples was not so much the growth of the nanoparticles but the enhancement of their stability in aqueous dispersion, as we will be see below. The better definition of particle shape achieved with increasing holding time favoured the electrostatic repulsion and/or steric hindrance, and thus the stabilization of the suspensions. In similar hydrothermal procedures with sodium polyacrylate as additive[22] an evolution of particle shape with time (within 168 h.) from platelets to fibres has been reported. Unlike the observed in the present work, authors noticed a decrease in pH values during hydrothermal aging that may be the cause of the morphological transformation. As it has been establish in the literature[34, 35] pH strongly affects the morphology of boehmite particles, favouring elongated shapes with decreasing pH values.

X-ray diffraction and HRTEM microstructural analysis

XRD patterns of the precipitated boehmite solid (xerogels) obtained with and without additives are shown in Figure 2S. Broader peaks with lower intensities were observed for M and T xerogels compared to the additive-free sample. Figures 3S, 4S and 5S display the set of XRD patterns prior and after the hydrothermal processing at different temperatures and time periods of gels without additive, with tartaric acid and maltitol, respectively. It can be seen that diffractograms corresponding to even short time hydrothermally processed boehmite xerogels showed sharper and more intense diffraction peaks than the starting materials. This fact can be associated with the improving of crystallinity and/or the presence of much larger crystallites. A preferred orientation effect evidenced by the high

relative intensity of the diffraction peak (020) is clearly observed in the diffraction patterns, indicating the presence of certain texture in the material, consequence of a particle shape with high aspect ratio, as was previously determined by TEM measurements. This effect is more pronounced in the additive-free hydrothermally treated material due to its more developed particle growth. It is to be noted that the differences observed in the XRD patterns of additive-free and with additive xerogels remained after hydrothermal treatment. Thus, additive-free samples always showed narrower profiles with higher peak intensities than materials prepared in the presence of tartaric acid or maltitol, which showed, in that order, increasing broadening of their diffraction profiles. An example of these differences is represented in Figure 2, in which the xerogels were processed at 200 ºC for 168 h.

Assuming that the prepared boehmites reached high crystallinity, it would be possible to evaluate their microstructure from the performed XRD experiments. The simpler methodology is the application of the Scherrer method, with an estimation of the instrumental broadening by means of a standard, (LaB_6). The main purpose of the crystallite size determination was to compare the trend of the variation of these estimated crystallite sizes to the trend of nanoparticle size measured from TEM micrographs.

Regarding these microstructural modifications, the analysis of samples prepared at 200 ºC clearly showed the effects of hydrothermal treatment and of the presence of additive in the final materials. As a representative comparison the three materials obtained at 200ºC for 168 h displayed in Figure 2 can be considered. Table 2 summarizes the measured position of the basal reflection (020), its full width at half maximum and the crystallite size (<Dv>) calculated using the Scherrer equation for the [020] crystallographic direction for all samples prepared at 200 ºC. The largest crystallite sizes were observed in samples prepared without additive. In samples prepared in the presence of tartaric acid reductions

in crystallite size for [020] directions with respect to additive-free materials reached 60% for 168 h. Decrease in [020] crystallite size was greater in the case of samples prepared with maltitol, showing reduction percentages of up to 80 % for 168 h holding time. Calculated [020] crystallite sizes matched the corresponding particle thicknesses values (**e**, Table 1) obtained from TEM measurements of the analysed samples. This correspondence supported the methodology employed in the size determinations on TEM images, assessing its suitability.

Although small in size, evidences of well-developed crystalline structures were found in the well-defined morphology of the particles observed by TEM as well as in their X-ray diffraction profiles, where the observed profile broadening found its main cause in the reduction of size of the coherent diffraction domains as a consequence of the reduction in particle size, which reached a factor of 6 when comparing the extreme size values in Table 2. An important factor related to the crystallinity of the boehmite, widely discussed in the literature, is the increase in the 020 interplanar distance. Its consequence, the shift of the 020 reflection position to lower angles in the diffraction profile, sometimes in the range of units of º2θ[36], aroused some controversy in the literature[37]. It was previously attributed to the presence of interlayer water[38] and afterwards to a relaxation of the attractive forces between layers due to the effect of peripheral absorption of water[40]. Subsequent studies established the small number of octahedral layers in finely crystalline boehmite as the main reason for this shift, although both the d(020) displacement and its profile broadening were enhanced by interlayer molecules of water[36]. Considering this, the occurrence of finer crystalline boehmite in the presence of additive is also supported by the observed slight d(020) increase (in the order of tenths of º2θ, as resumed in Table 2)[14] when compared with the 2θ positions obtained in the preparation without additive. The relatively small

d(020) shifts suggests the presence of well-ordered crystalline structure in small coherent diffraction domains.

HRTEM observations confirmed the well-developed crystallinity of the nanoparticles, formed by single crystals with clearly visible interplanar distances. As a representative example, in Figure 6S is shown a set of boehmite nanoparticles with different orientations constituted by single crystalline domains.

Elemental analysis

In order to assess the presence of additives in the final powder, elemental analysis determinations were carried out in samples 0_200_168, T_200_168 and M_200_168. Table 3 resumes the weight percentage of N, C and H determined for the three materials. A significant amount of carbon was detected in sample prepared with maltitol, whereas low, negligible C content values were found for preparations without additive or with tartaric acid. This result allowed establishing that no carbon from tartaric acid is present in the dry powder obtained by the preparation with this additive. Thus, unlike the proposed for maltitol, surface interaction with boehmite nanoparticles is discarded. As was mentioned above, particles obtained in the presence of tartaric acid showed smaller size but similar aspect ratio than those obtained without additive. This may point to a slower, surface interaction-free growth of the boehmite nanoparticles, equivalent to that of samples prepared without additive.

Characterization of aqueous suspensions of boehmite nanoparticles

The stability of boehmite nanoparticles in aqueous dispersions is an important feature for many of their applications. Measurements of PSDs and ζ-potential of the aqueous suspensions of the nanoparticles obtained in this study help in the characterization of their stability.

Aqueous suspensions of materials prepared at 150 and 200 ºC for 24h, illustrative of the behaviour of rest of the materials, exhibited the PSDs plotted in Figure 3. Although the achieved dispersion was enough to perform the DLS measurements properly, suspensions presented some degree of particle aggregation. This leaded to the disagreement between the TEM and DLS size estimations.

Considering the effect of additives, it was observed that for all cases, dispersion efficiency was higher in samples prepared with maltitol, which showed the particle distributions of smaller sizes. Increasing the treatment temperature enhanced the stabilization effect of maltitol, as can be observed in the comparison of Figure 3. Only in M-containing samples fundamental particles –i.e., with sizes corresponding to the TEM observations- were detected. Materials prepared with tartaric acid or without additive presented a larger proportion of aggregates [22] that shifted the distribution towards bigger particle sizes. Nanoparticles prepared with tartaric acid improved their dispersion with respect to the additive-free obtained materials when the hydrothermal treatment proceeded at 200 ºC. Nanoparticles obtained at this temperature in the presence of additive showed a remarkable enhancement of their dispersion ability in aqueous suspension, clearly noticed in Figure 3B. Holding time of hydrothermal treatment also influenced the behaviour of boehmite nanoparticles in aqueous suspensions. Figure 7SA and 7SB compare the PSDs of 24 and 168 h additive-free treated materials at 150 and 200 ºC respectively. For both temperatures, the samples treated during 168 h showed better dispersion, with PSD reaching lower size values.

Measurements of ζ-potential of as-prepared boehmite nanoparticles aqueous suspensions (pH=8.7) (Figure 4) also evidenced differences in the behaviour of samples depending on their preparation procedure. While no noticeable differences were observed in ζ-potential when working at 150 ºC (Figure 4B) samples prepared at 200 ºC exhibited increasing absolute values in the sequence 0_200_24 < T_200_24 < M_200_24 (Figure 4A). This pointed to an increment of the negative surface charge in materials prepared with additives, in good agreement with the enhanced dispersion and the consequent improvement of the stabilization of their aqueous suspensions observed in DLS determinations.

It is to be noted that the addition of maltitol molecules in the preparation of boehmite presented a double effect on the stabilization of its aqueous suspensions. On one side, the higher proportion of negatively charged lateral faces increased the surface charge of the particles as was clearly established by ζ-potential measurements (Figure 4). On the other side, detection of significant carbon content through elemental analysis of the final product obtained with maltitol addition (Table 3) pointed to the presence of relatively big molecules of maltitol anchored in the lateral surfaces of the particles, inducing a steric hindrance effect. Both consequences of the use of maltitol helped the repulsion between boehmite nanoparticles, allowing a better dispersion that resulted in the increase of the stability of their aqueous suspensions, as supported by DLS and ζ-potential determinations. Indeed, the balanced combination of electrostatic repulsion with steric stabilization was reported as optimal for the stabilization of highly concentrated suspensions of alumina[41].

As lateral faces are responsible of the surface charge, nanoparticles prepared in the presence of tartaric acid at 200 ºC showed a slight increase in their ζ-potential absolute value, as presented in Figure 4. This effect is not as pronounced as in the case of maltitol, where an effective change in the shape of the nanoparticles (aspect ratio) was achieved. Still, the effect of tartaric acid in the preparation of boehmite nanoparticles was enough to

enhance the dispersion of the material (Figure 3B) and the stability of their aqueous suspension.

Remarks on the role of additives

From the results obtained it can be inferred that both additives used, tartaric acid and maltitol, play a quite different role in both the precipitation step and in the subsequent hydrothermal aging, leading to a variety of final properties in the boehmite preparation. For the sake of clarity Table 4 summarizes the main morphological characteristics of the boehmite nanoparticles prepared together with their crystallinity and stability of their aqueous dispersions.

It is proposed that tartaric acid slow down the boehmite formation due to the ability of tartrate anions to coordinate Al^{3+} to form tartrate-aluminium complexes. On the contrary, the capability of maltitol to coordinate Al^{3+} is negligible and its effect is based on its interaction with the lateral surfaces of the solid. Thus, action of tartaric acid is related to the rate of nucleation and growth of the nanoparticles, while maltitol affects their surface chemistry, hindering the condensation of nuclei and modifying their morphology development. Both additives, thus, extend their effect to the whole preparation process.

In general, hydrothermal aging involves different mechanisms in the transformations of nanoparticles. When the nanoparticles are partially soluble, the concentration of chemical species in solution may be high enough to nucleate a more stable crystalline phase; then the formation of well crystallized particles take place by a slow dissolution-recrystallization process. Such a process leads to a new crystalline phase, which was not observed in the present study.

Solubility of boehmite nanoparticles is very low, so the crystallization of the early amorphous or poorly crystallized solid can only proceed by an in situ solid state transformation. This transformation involves diffusion of ions within the solid as well as partial dehydration.

Main morphological differences between the three types of boehmite were mostly induced in the precipitation process; in the case of tartarte-containing samples controlling the nucleation and growth rate and in the maltitol system by the stabilization by adsorption of maltitol molecules on lateral faces of the early developed nuclei. Hydrothermal aging, on the other hand, increased the crystallinity of the nanoparticles as assessed by XRD, enhancing properties as aqueous dispersion stability.

Conclusions

A procedure to control the size and shape and to improve the dispersability in aqueous media of boehmite nanoparticles synthesized by a hydrothermal via is reported. Free-additive and tartaric- and maltitol-containing xerogels previously obtained from a solution of aluminum nitrate at pH 10 were hydrothermally treated at 150 and 200 ºC for times between 24 h and 168 h. Higher hydrothermal treatment temperature and time resulted in the increase of average particle size and in the broadening of size distributions.

On the contrary, the presence of additives in the hydrothermal process led to both a size reduction between 40 and 70 % and narrower particle size distributions. In addition, some shape changes were also enabled.

With respect to the aqueous dispersion stability, it was found that the longer stabilities were observed for samples prepared in the presence of additive, being the longest the maltitol-grafted boehmite nanoparticle dispersions, with hydrodynamic sizes of around 50-60 nm. Hydrothermal aging time was found to increase the water dispersability of the materials.

Finally, it is to be remarked that in this work a quantitative evaluation of the size and particle size distribution from the analysis of TEM images has been reported.

Acknowledgements

Financial support from the Spanish Ministry of Economy and Competitiveness through project CONSOLIDER INGENIO 2010 CSD2010-00065 is acknowledged.

Technical support from the Servei Central de Suport a l'Investigació Experimental (SCSIE) of the University of Valencia in the application of TEM and XRD techniques is also acknowledged.

References

1 M. Li, B. Lebeau and S. Mann, *Adv. Mater.,* 2003, **15**, 2032.

2 Y. Xia, P. Yang, Y. Sun, Y. Wu, B. Mayers, B. Gates, Y. Yin, F. Kim and H. Yan, *Adv. Mater*,. 2003, **15**, 353.

3 J. Yang, Z. Quan, D. Kong, X. Liu and J. Lin, *Cryst. Growth Des*., 2007, **7**, 730.

4 M. Digne, P. Sautet, P. Raybaud, P. Euzen and H. Toulhoat, *J. Catal*., 2002, **211**, 1.

5 M. Digne, P. Sautet, P. Raybaud, P. Euzen and H. Toulhoat, *J. Catal*., 2004, **226**, 54.

6 M. Amoura, N. Nassif, C. Roux, J. Livage and T. Coradin, *Chem. Commun*., 2007, 4015.

7 R. Aucejo, J. Alarcón, C. Soriano, M. C. Guillem, E. García-España and F. Torres, *J. Mater. Chem*., 2005, **15**, 2920.

8 E. Delgado-Pinar, J. C. Frías, L. J. Jiménez-Borreguero, M. T. Albelda, J. Alarcón and E. García-España, E. *Chem. Commun*., 2007, 3392.

9 A. Rutenberg, V. V. Vinogradov and D. Avnir, *Chem. Commun*., 2013, **49**, 5636.

10 S. Musić, Đ. Dragčević and S. Popović, *Mater. Lett*., 1999, **40**, 269.

11 M. Nguefack, A. F. Popa, S. Rossignol and C. Kappenstein, *Phys. Chem. Chem. Phys*., 2003, **5**, 4279.

12 X. Bokhimi, J. A. Toledo-Antonio, M. L. Guzmán-Castillo and F. Hernández-Beltrán, *J. Solid State Chem*., 2001, **159**, 32.

13 K. Okada, T. Nagashima, Y. Kameshima, A. Yasumori and T. Tsukada, *J. Colloid Interface Sci*., 2002, **253**, 308.

14 J. Sánchez-Valente, X. Bokhimi and F. Hernández, *Langmuir*, 2003, **19**, 3583.

15 T. Tsukada, H. Segawa, A. Yasumori, and K. Okada, *J. Mater. Chem*., 1999, **9**, 549.

16 D. Chiche, C. Chanéac, R. Revel and J. P. Jolivet, *Phys. Chem. Chem. Phys*., 2011, **13**, 6241.

17 D. Chiche, C. Chizallet, O. Durupthy, C. Chanéac, R. Revel, P. Raybaud and J. P. Jolivet, *Phys. Chem. Chem. Phys*., 2009, **11**, 11310.

18 T. He, L. Xiang and S. Zhu, *Langmuir*, 2008, **24**, 8284.

19 B. Dash, B. C. Tripathy, I. N. Bhattacharya and B. K. Mishra, *Dalton Trans*., 2010, 39, 9108.

20 H. Y. Zhu, J. D. Riches and J. C. Barry, *Chem. Mater*., 2002, **14**, 2086.

21 Y. Mathieu, B. Lebeau and V. Valtchev, *Langmuir*, 2007, **23**, 9435.

22 Z. Zhang and T. J. Pinnavaia, *J. Am. Chem. Soc*., 2002, **124**, 12294.

23 S. Musić, Đ. Dragčević and S. Popović, *Mater. Lett*., 1995, **24**, 59.

24 P. A. Buining, C. Pathmamanoharan, M. Bosboom, J. B. H. Jansen and H. N. W. Lekkerkerker, *J. Am. Ceram. Soc*., 1990, **73**, 2385.

25 T. Tsuchida, *J. Eur. Ceram. Soc*., 2000, **20**, 1759.

26 C. Kaya, J. Y. He, X. Gu and E. G. Butler, *Microporous Mesoporous Mater*., 2002, **54**, 37.

27 S. Musić, Đ. Dragčević, S. Popović and A. Turković, *Mater. Lett*., 1994, **18**, 309.

28 B. E. Yoldas, *J. Appl. Chem. Biotechnol*., 1973, **23**, 803.

29 J. P. Jolivet, S. Cassaignon, C. Chanéac, D. Chiche and E. Tronc, *J. Sol-Gel Sci. Technol*., 2008, **46**, 299.

30 M. Moreaud, D. Jeulin, V. Morard and R. Revel, *J. Microsc*., 2012, **245**, 186.

31 G. K. Ambady and G. Kartha, *Acta Cryst*., 1968, **B24**, 1540.

32 S. Desroches, S. Daydé and G. Berthon, *J. Inorg. Biochem*., 2000, **81**, 301.

33 E. Marklund and L. O. Öhman, *J. Chem. Soc*., *Dalton Trans*., 1990, 755.

34 J. P. Jolivet, C. Chanéac, D. Chiche, S. Cassaignon, O. Durupthy and J. Hernandez, *C. R. Geosci*., 2011, **343**, 113.

35 X. Y. Chen, H. S. Huh and S. W. Lee, S. W. *Nanotechnology*, 2007, **18**, 285608.

36 X. Y. Chen, Z. J. Zhang, X. L. Li and S. W. Lee, *Solid State Commun.*, 2008, **145**, 368.

37 R. Tettenhorst and D. A. Hofmann, *Clays Clay Miner.*, 1980, **28**, 373.

38 P. Alphonse and M. Courty, *Thermochim. Acta*, 2005, **425**, 75.

39 D. Papee, R. Tertian and R. Biais, *Bull. Soc. Chim. Fr.*, 1958, 1301.

40 B. R. Baker and R. M. Pearson, *J. Catal.*, 1974, **33**, 265.

41 L. Palmqvist, O. Lyckfeldt, E. Carlström, P. Davoust, A. Kauppi and K. Holmberg, *Colloids Surf., A*, 2006, **274**, 100.

Table 1. Descriptive parameters of particle size distributions as measured on TEM images. **L**, average length of major diagonal of the platelets; $\mathbf{s_L}$, *L* standard deviation; $\mathbf{M_L}$, mode of L; $\mathbf{FWHM_L}$, full width at half maximum of L distribution; $\mathbf{n_L}$, number of length measurements; **e**, average thickness of the particles; $\mathbf{s_e}$, *e* standard deviation; $\mathbf{n_e}$, number of thickness measurements; **r**, aspect ratio (e/L).

Sample	L (nm)	s_L (nm)	M_L (nm)	$FWHM_L$ (nm)	n_L	e (nm)	s_e (nm)	n_e	r
0_150_24	21.1	10.6	14.43	13.3	115	5.2	3.0	68	4.0
T_150_24	21.2	11.3	12.12	17.4	142	4.9	1.0	95	4.3
M_150_24	15.4	5.3	9.0	11.8	224	4.7	1.1	108	3.3
0_150_168	32.8	13.9	22.1	26.5	90	4.7	1.7	65	7.0
T_150_168	28.7	11.3	19.3	16.5	93	5.8	1.4	38	4.9
M_150_168	10.7	3.7	7.9	9.5	48	3.7	1.1	38	2.9
0_200_24	69.6	24.0	63.1	53.9	96	15.9	5.7	20	4.4
T_200_24	41.9	13.3	28.2	22.9	136	9.6	1.9	44	4.4
M_200_24	15.8	6.2	14.2	16.7	194	4.8	4.8	85	3.3
0_200_168	94.7	30.5	76.0	51.34	120	25.2	6.0	19	3.8
T_200_168	59.4	24.2	36.4	39.33	169	14.0	2.8	40	4.2
M_200_168	17.6	10.3	6.3	10.42	121	7.5	1.9	120	2.3

Table 2. Position (**Pos.**), Full Width at Half Maximum (**FWHM**) and crystallite size (**<Dv>**) obtained from (020) diffraction profile of materials prepared at 200ºC.

Sample	Pos. (º2θ)	FWHM (º2θ)	<Dv> (nm)
0_200_24	14.424	0.366	13.8
0_200_72	14.420	0.260	23.4
0_200_168	14.436	0.238	33.1
T_200_24	14.292	0.653	10.5
T_200_72	14.317	0.585	12.4
T_200_168	14.328	0.541	13.1
M_200_24	14.346	1.053	5.0
M_200_72	14.380	1.011	6.5
M_200_168	14.340	0.950	7.2

Table 3. Elemental analysis of final powders.

Sample	N (wt. %)	C (wt. %)	H (wt. %)
0_200_168	0.11	0.05	1.35
T_200_168	0.05	0.04	1.91
M_200_168	0.11	0.95	1.72

Table 4. Summary of the main features of the prepared boehmites.

Sample	Shape	L (nm)	e (nm)	$<Dv>_{020}$ (nm)	Aqueous Stability	ζ (mV)
0_150_24	Square	21.1	5.2	-	low	-21.6
T_150_24	Square	21.2	4.9	-	low	-18.4
M_150_24	Square	15.4	4.7	-	high	-17.4
0_150_168	Rhombic	32.8	4.7	-	low	-
T_150_168	Square	28.7	5.8	-	low	-
M_150_168	Square	10.7	3.7	-	high	-
0_200_24	Rhombic	69.6	15.9	13.8	low	-
T_200_24	Square	41.9	9.6	10.5	medium	-
M_200_24	Square	15.8	4.8	5.0	high	-
0_200_168	Rhombic	94.7	25.2	33.1	low	-12.4
T_200_168	Rhombic	59.4	14.0	13.1	medium	-17.8
M_200_168	Square	17.6	7.5	7.2	high	-24.4

Figure captions

Figure 1. TEM micrographs of samples prepared in this work: 0_150_24 (A), T_150_24 (B), M_150_24 (C), 0_150_168 (D), T_150_168 (E), M_150_168 (F), 0_200_24 (G), T_200_24 (H), M_200_24 (I), 0_200_168 (J), T_200_168 (K), M_200_168 (L). Scale bar is 100 nm except for B (20 nm) and J, K and L (200 nm).

Figure 2. Powder X-ray diffraction patterns of samples prepared at 200 ºC for 168 h without additive, with tartaric acid and with maltitol. Bars indicate the position and relative intensity of boehmite reflections (Ref. Code: 00-005-0190).

Figure 3. Particle size distributions of samples treated at 150 ºC for 24 h (A) and at 200 ºC for 24 h (B) determined by DLS.

Figure 4. Determination of ζ-Potential at pH 8.7 for samples 0, T and M prepared at (A) 200 ºC for 168 h and (B) at 150 ºC for 24 h.

Figure 1. TEM micrographs of samples prepared in this work: 0_150_24 (A), T_150_24 (B), M_150_24 (C), 0_150_168 (D), T_150_168 (E), M_150_168 (F), 0_200_24 (G), T_200_24 (H), M_200_24 (I), 0_200_168 (J), T_200_168 (K), M_200_168 (L). Scale bar is 100 nm except for J, K and L (200 nm).

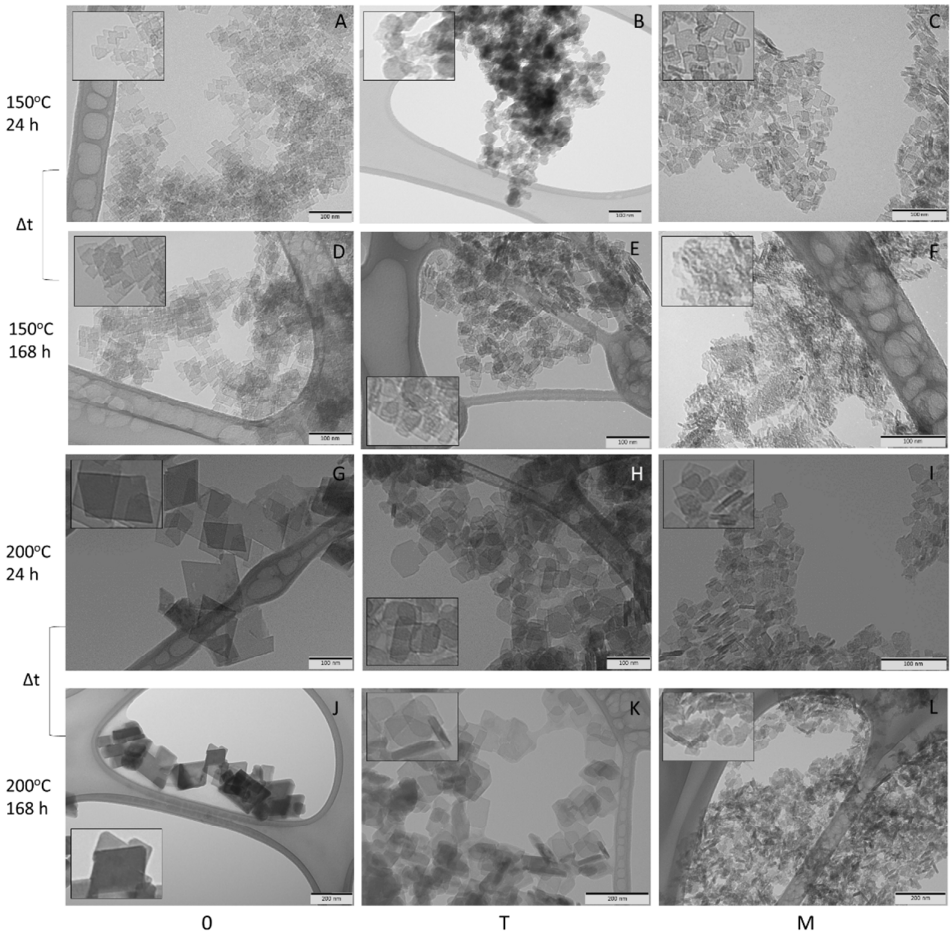

Figure 2. Powder X-ray diffraction patterns of samples prepared at 200 ºC for 168 h without additive, with tartaric acid and with maltitol. Bars indicate the position and relative intensity of boehmite reflections (Ref. Code: 00-005-0190)

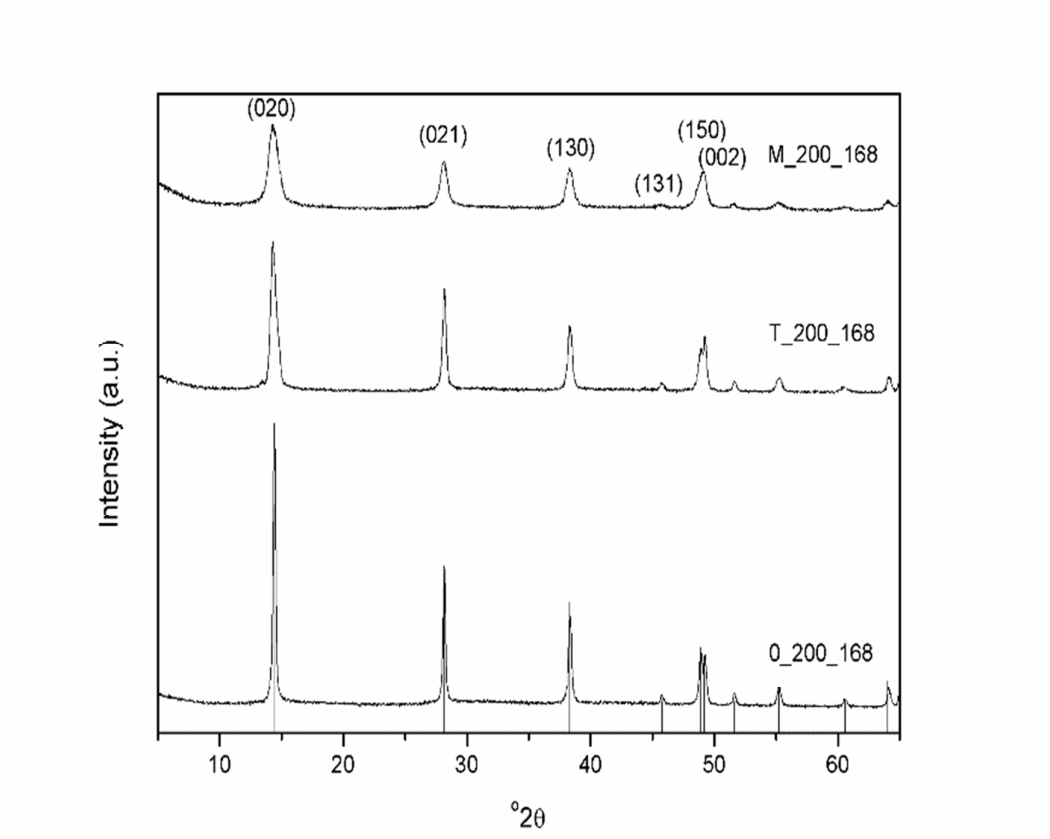

Figure 3. Particle size distributions of samples treated at 150 ºC for 24 h (A) and at 200 ºC for 24 h (B) determined by DLS.

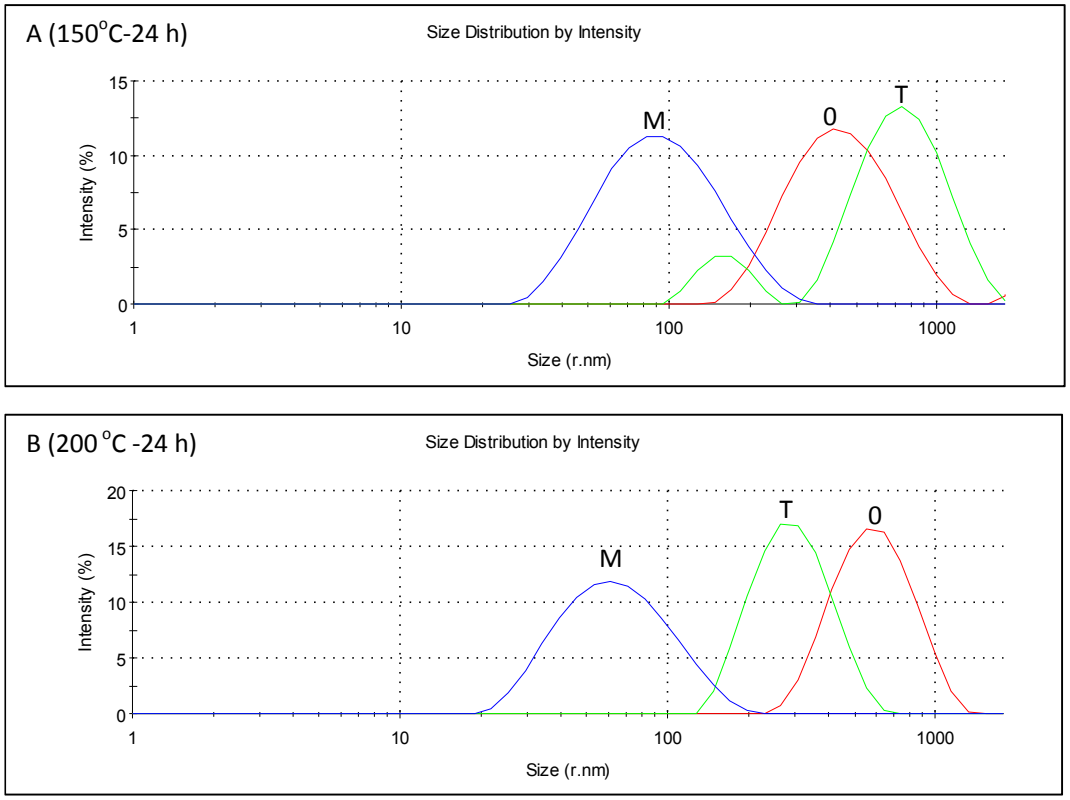

Figure 4. Determination of ζ-Potential at pH 8.7 for samples 0, T and M prepared at (A) 200 ºC for 168 h and (B) at 150 ºC for 24 h.

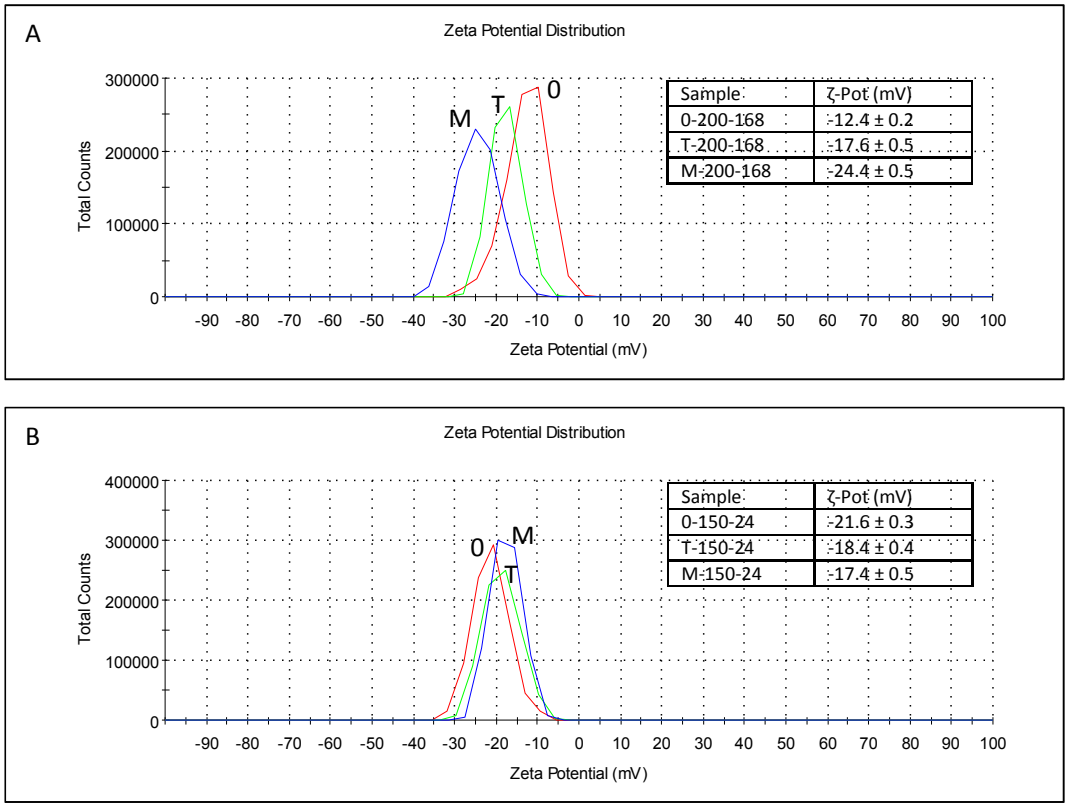

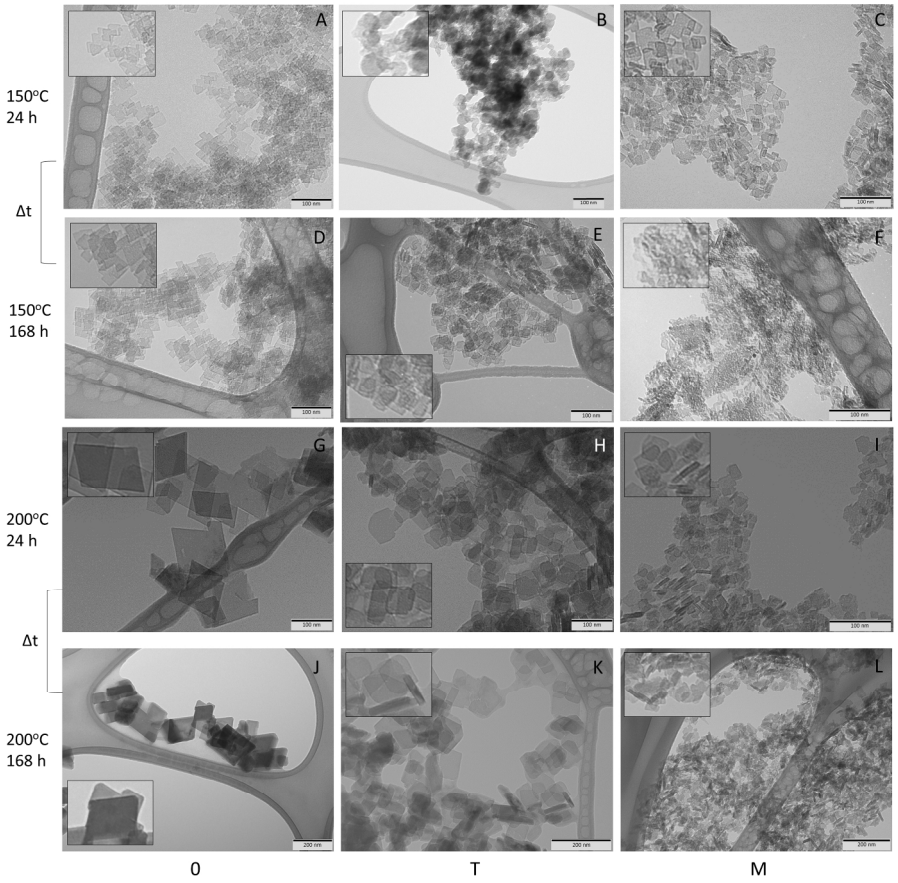

Figure 1. TEM micrographs of samples prepared in this work: 0_150_24 (A), T_150_24 (B), M_150_24 (C), 0_150_168 (D), T_150_168 (E), M_150_168 (F), 0_200_24 (G), T_200_24 (H), M_200_24 (I), 0_200_168 (J), T_200_168 (K), M_200_168 (L). Scale bar is 100 nm except for B (20 nm) and J, K and L (200 nm).
626x699mm (96 x 96 DPI)

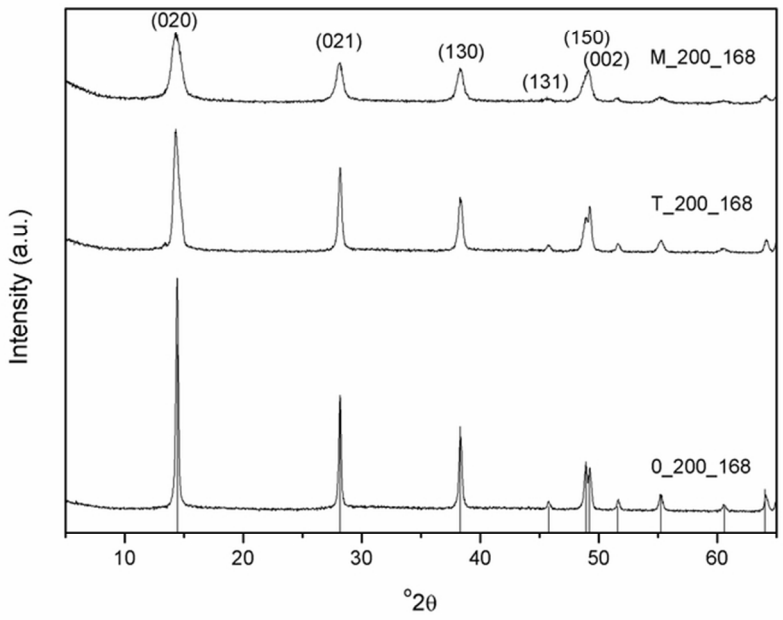

Figure 2. Powder X-ray diffraction patterns of samples prepared at 200 ºC for 168 h without additive, with tartaric acid and with maltitol. Bars indicate the position and relative intensity of boehmite reflections (Ref. Code: 00-005-0190).
70x49mm (300 x 300 DPI)

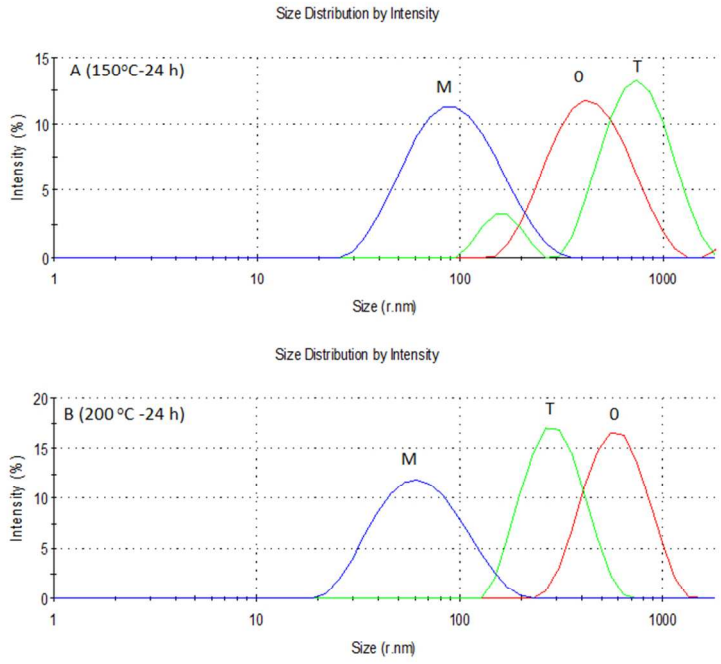

Figure 3. Particle size distributions of samples treated at 150 ºC for 24 h (A) and at 200 ºC for 24 h (B) determined by DLS.
250x179mm (96 x 96 DPI)

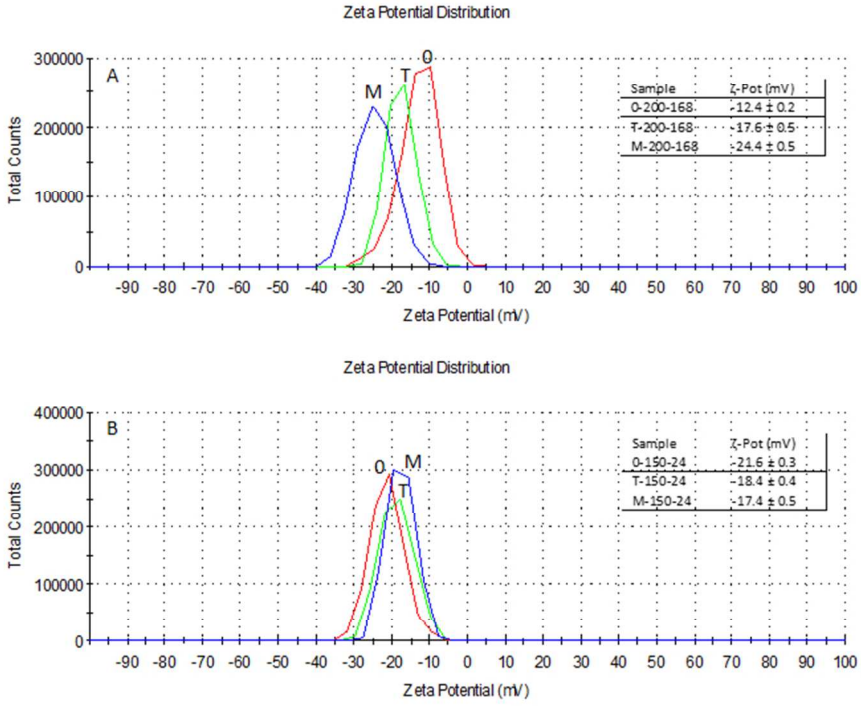

Figure 4. Determination of ζ-Potential at pH 8.7 for samples 0, T and M prepared at (A) 200 ºC for 168 h and (B) at 150 ºC for 24 h.
200x150mm (96 x 96 DPI)